Nuclear Science and Techniques (2025) 36:184
https://doi.org/10.1007/s41365-025-01747-8

Selective removal of Be(II) from uranium–beryllium-containing solutions via a green chelate-like phosphate-based adsorbent functionalized by glycine composite: experimental and DFT investigations

Xu Zhao[1] · E-Ming Hu[2] · Yi-Ge Sun[3] · Hao-Shuai Li[2] · Hong Liu[4] · Zhi-Wu Lei[2] · Yu-Cheng Su[2] · Bo-Yuan Zheng[2] · Hong-Yang Xia[2] · Khan-Muhammad-Yaruq Ali[2] · Qing-Liang Wang[2] · Fang Hu[2]

Received: 6 June 2024 / Revised: 30 July 2024 / Accepted: 10 August 2024 / Published online: 18 July 2025

Abstract

A green chelate-like phosphate-based adsorbent functionalized by glycine (CP@Glycine) was first designed, synthesized, and applied to selectively separate Be(II) from uranium–beryllium-containing (U/Be) solutions. The optimal adsorption conditions were: $W_{H_3PO_4}/W_{Ca(OH)_2}/W_{Glycine}$ (wt/wt/wt) of 3:3:1, pH=6, resulting in the maximum adsorption efficiency of 99% in the case of adsorbent of 2 g · L^{-1}. CP@Glycine exhibited excellent selectivity for Be(II) ($K_d = 2.53 \times 10^4$ mL · g^{-1}) toward Fe, U, Zn, Mn, Na, and Ca in solutions. After 5 adsorption–desorption cycles, the removal efficiency of Be(II) remained at 85%, and the desorption rate of Be(II) was above 90%. Adsorption kinetics and thermodynamics studies showed that the theoretical maximum adsorption capacity (Q_e) of CP@Glycine was 66 mg · g^{-1}, which was higher than the state-of-the-art adsorption materials. Besides, the surface of CP@Glycine exhibited abundant active sites with negative charges which would have a potential electrostatic attraction with Be(II). Moreover, the adsorption mechanism of CP@Glycine was methodically revealed through a combination of various characterizations and DFT investigations. It was found that $BeNH_4PO_4$ and $Be(OH)_2$ were formed as stable precipitates on the surface of CP@Glycine, which implied that Be(II) was coordinated with the amino and the phosphate groups from CP@Glycine, thus achieving the chelation effect of Be(II) with CP@Glycine for the adsorption process. The results of DFT investigations further confirmed that Be(II) owned strong bonding affinity to the amino group and the phosphate group from the as-prepared CP@Glycine. The results indicated that the calculated binding energy of the Be complex coordinated with glycine and phosphate (−229.37 kcal · mol^{-1}) was lower than that of other possible Be complexes. The above findings revealed that CP@Glycine could be a promising adsorbent for the selective separation and recovery of Be(II) from U/Be wastewater.

Keywords Adsorption · Selectivity · $BeNH_4PO_4$ · $Be(OH)_2$ · Desorption

1 Introduction

As a critical rare material, beryllium is extensively utilized in alloys, electronics, and computer industries [1, 2]. Currently, the total resources of beryllium in the world

This work was supported by the National Key R&D Program of China (No.2023YFC2907802). The National Natural Science Foundation of China (52204363). The Research Project of Hunan Provincial Education Department of China (No. 22B0440). The calculation process is based on the High-Performance Computing Center of Central South University. Test data provided by Luobo Lab (www.luobolab.com).

✉ Qing-Liang Wang
670566869@qq.com

✉ Fang Hu
csuhufang@163.com

[1] School of Nuclear Science and Technology, University of South China, Hengyang 421001, China

[2] School of Resource Environment and Safety Engineering, University of South China, Hengyang 421001, China

[3] College of Resources and Environment, Anhui Agricultural University, Hefei 230000, China

[4] School of Metallurgy and Environment, Central South University, Changsha 410000, China

are about 3.383million tons, and proven mineral reserves account for 1.164 million tons [3]. Beryllium is listed by the European Union as one of the 14 most critical mineral resources [4]. With the increasing demand for beryllium in the world and the continuous increase in mineral resources exploitation, the mining geological environment has been increasing concern by government and investigators because of the extremely high toxicity of beryllium. Several investigators reported that Be(II) migrated easily into the environment, mainly through ore mining, weathered rocks and minerals, and coal pile leaching [5–7]. Hence, beryllium would inevitably migrate from mineral resources to water resources to produce substantial quantities of wastewater containing beryllium. It is well known that beryllium is a highly toxic metal, and humans exposed to beryllium for long periods are susceptible to beryllium lung disease and cancer [8]. Additionally, beryllium would also contaminate agricultural ecosystems and seriously disrupt the growth of crops [9, 10]. WHO displays that the maximum allowable limit for beryllium wastewater discharge would be 0.012 $mg \cdot L^{-1}$ (Guidelines for Drinking-Water Quality). Therefore, the treatment of U/Be wastewater has become more and more urgent. On the other hand, there exist many metal cations (Zn(II), Mn(II), Ca(II), Fe(II), Na(I), and (VI)) in U/Be wastewater, which would affect the removal of Be(II) [8]. As a result, the selective separation of Be(II) from U/Be solutions is very challenging due to the low concentration and coexistence of multiple ions.

At present, the treatment of U/Be wastewater is mainly performed by adsorption, precipitation, and biological approaches. Among them, adsorption is the optimal methodology due to its advantage in purifying solutions with low concentrations. Sun et al. [11] found that activated sludge could adsorption Be(II) from U/Be solutions and the reported adsorption capacity Q_e value of the activated sludge was 14.4 $mg \cdot g^{-1}$. Mahmoud et al. [12] employed chitosan to adsorb Be(II) and the Q_e of chitosan was 44.96 $mg \cdot g^{-1}$. Zhao et al. [13, 14] utilized modified biochar for the treatment of U/Be wastewater and reached maximum adsorption capacity Q_e (45.68$mg \cdot g^{-1}$ and 32.86 $mg \cdot g^{-1}$) under neutral conditions. In conclusion, the adsorbents currently reported for Be(II) generally have a Q_e of lower than 50mg/g. The low adsorption capacity and economics of the reported adsorbents limited their application. Therefore, the design and preparation of economical and environmentally sound adsorbents with high selectivity and adsorption capacity are crucial for the treatment of U/Be wastewater.

Previous investigations [15, 16] revealed that Be(II) exhibited a strong coordination property with hard O donor atoms. De and Krishnamoorthy [17, 18] reported that Be(II) is capable of forming stable complexes with phosphate and ammonia to produce precipitation. On the other hand, it is well known that the N, O, and S donor atoms in the carbon side chains of amino acids can be considered as active sites. Owing to the excellent complexation ability of amino acids, Sarvar et al. [19] utilized eight amino acids for gold leaching. Considering the strong coordination affinity of Be(II) with the N donor atom, this paper aims to propose the possibility of constructing a phosphate-based adsorbent functionalized by amino acid for the selective adsorption of Be(II) from U/Be solutions in an innovative way.

In this paper, a green, energy-saving, and efficient adsorption material with high selectivity is prepared for the removal of beryllium toward impurity ions from the aspect of functional group design. To the best of our knowledge, this is the first time for an amino acid to be utilized as an adsorbent. Before this, phosphates were broadly utilized for the determination of beryllium [17, 18], and the results showed that phosphate has a strong binding ability to beryllium. Therefore, we speculate that phosphate can be effectively employed for the removal of beryllium from the solution. The main concept of the present investigation is to design and prepare an effective adsorbent via one kind of amino acid and calcium phosphate, which provide nitrogen and phosphorus sources for the coordination of Be(II). The crucial goal is to achieve the selective removal of beryllium from U/Be solutions. The removal and separation behaviors of Be(II) from U/Be solutions with the as-prepared absorbent material (named as CP@Glycine) were examined by using batch experiments. The adsorption thermodynamics and kinetics of Be(II) with CP@Glycine were also determined. Besides, the adsorption selectivity of Be(II) toward Fe(II), U(VI), Zn(II), Mn(II), Na(I), and Ca(II) was also methodically explored. The removal mechanism was thoroughly investigated by the combination of different characterizations. At the same time, the adsorption capacity of CP@Glycine is 66 $mg \cdot g^{-1}$, which is higher than the largest known adsorbent ($Q_e = 55\,mg \cdot g^{-1}$) [15]. In addition, DFT investigations were used in this study to explore the possible coordination interactions between Be(II) and the ligands from CP@Glycine. Based on the above studies, a novel environmentally sound beryllium separation technology would be established and the adsorption mechanism would be discovered at atomic level.

2 Experiment

2.1 Materials

Glycine (Gly) ($C_2H_5NO_2$, purity: 99%, CAS Number: 56-40-6), $ZnCl_2$ (purity: 98%, CAS Number: 7646-85-7), $MnSO_4.H_2O$ (purity: 98%, CAS Number:

10034-96-5), $FeSO_4$ (purity: 90%, CAS Number: 10034-96-5), $CaCl_2$ (purity: 96%, CAS Number: 10043-52-4), NaCl (purity: 99%, CAS Number: 7647-14-5), phosphoric acid (H_3PO_4, purity: 85%, CAS Number: 7664-38-2), BeO (purity: 99%, CAS Number: 1304-56-9), $Ca(OH)_2$ (purity: 99%, CAS Number: 1305-62-0) were purchased from China Shanghai McLean Biochemistry Co., Ltd.

2.2 Preparation of CP@Glycine

The CP@Glycine was prepared by the following procedure. 1 g of glycine was dissolved in 25 mL of deionized water, and then, 1.5 g of calcium hydroxide was added to the mixture. After stirring at 65 °C for 2 h, 1.5 g of phosphoric acid was poured uniformly and the mixture was then rapidly mixed. The obtained uniform solution was heated in an oven at 105 °C to dry and turn into a powder. The CP@Glycine powder prepared in this way was mostly used to remove Be(II) in U/Be solutions.

The preparation process of the adsorbent does not produce any toxic and harmful gases and can efficiently remove beryllium from ing wastewater.

2.3 Solution preparation

nd phosphoric acid in ord

roxide, and phosph

According to previous stud usually contains various elem Mn(II), Ca(II), Fe(II), Na(I), and U(VI). In th investigation, U/Be solutions with low conc (5 mg · L^{-1} and 10 mg · L^{-1}) were appropriately prepared for batch experiments, adsorption kinetics, and thermodynamic studies, whereas mixed solutions containing Be, Zn, Mn, Ca, Fe, Na, and U (10 mg · L^{-1}–50 mg · L^{-1}) were simulated for adsorption selectivity investigations.

2.4 Batch experimental analysis

The accuracy of results was demonstrated by the preparation of adsorbent, initial pH, amount of adsorbent, and adsorption of a simulated solution from U/Be solution. Three sets of parallel samples were utilized in batch experiments to verify the validity of the results. Batch test of $W_{H_3PO_4}/W_{Ca(OH)_2}/W_{Glycine}$ (wt/wt/wt) was conducted to investigate the effects of $W_{H_3PO_4}/W_{Ca(OH)_2}/W_{Glycine}$ =1:1:1, 2:2:1, 3:3:1, 4:4:1, 5:5:1 on the resulting adsorption. 0.05 g of five various substances was placed in a 50 mL solution to form a mixture. The mixture was placed in a shaking table under reaction conditions of 25 °C, 175 rpm, and 16 h. The mixture was then appropriately separated, and the concentration of Be(II) in the clarified solution was measured by an ultraviolet spectrophotometer (UV-2550, Shimadzu).

2.5 Adsorption kinetics and thermodynamics studies

0.1 g of CP@Glycine was weighed and placed in 50 mL beryllium solutions (C_0=10, 60, 180, 200, 220, 250, 300, and 350 mg · L^{-1}) and then divided into 8 groups with three parallel samples in each group. The above solutions were placed in a constant temperature shaking table and then oscillated at 175 rpm at three temperatures (i.e., 15 °C, 25 °C, and 35 °C) until arriving at the equilibrium. The adsorption kinetics of Be(II) were investigated with pseudo-first-order (PFO), pseudo-second-order (PSO), Elovich, and intraparticle diffusion models. The adsorption kinetics and thermodynamic models refer to the equation section entitled "Equations" in the Supporting Information.

2.6 Adsorption selectivity studies

The mixed solutions containing Be, Zn, Mn, Ca, Fe, Na, and · L^{-1}–50 mg · L^{-1}) were appropriately simulated orption selectivity studies. The selective adsorp- rmance of Be(II) from the solutions with CP@ as evaluated using the dispersion coefficient, K_d . The dispersion coefficient (K_d) can be calculated [21]:

$$K_d = \frac{(C_0 - C_e) \times V}{C_e \times m} \times 1000 \quad (1)$$

where C_e (mg · L^{-1}) is the equilibrium concentration; C_0 (mg · L^{-1}) is the initial concentration of Be. m (g) is the mass of the adsorbent. V (mL) is the solution volume.

3 Results and discussion

3.1 Characterization

Figure 1a demonstrates the SEM analysis diagram of CP@Glycine, from which it can be seen that CP@Glycine shows good agglomeration and irregular shape. Figure 1b shows the results of the TEM analysis. The original sample showed an irregular shape, and the average particle size of about 200 nm, CP@Glycine particle size greater than compared with separate calcium phosphate [22, 23] and amino acids. This result may be related to the presence of amino acids that alter the growth of calcium phosphate.

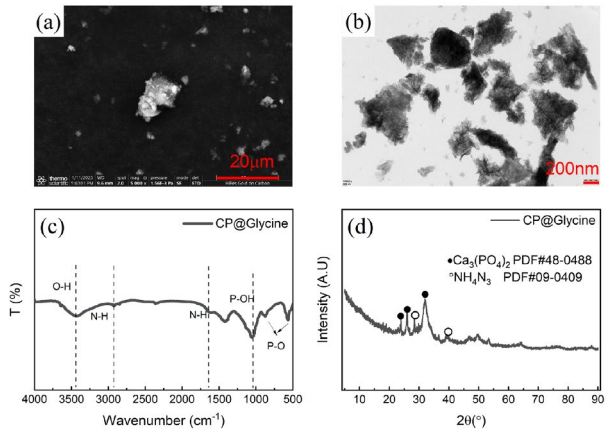

Fig. 1 (Color online) SEM analysis of CP@Glycine (**a**), TEM analysis of CP@Glycine (**b**), FT-IR analysis of CP@Glycine (**c**), XRD analysis of CP@Glycine (**d**)

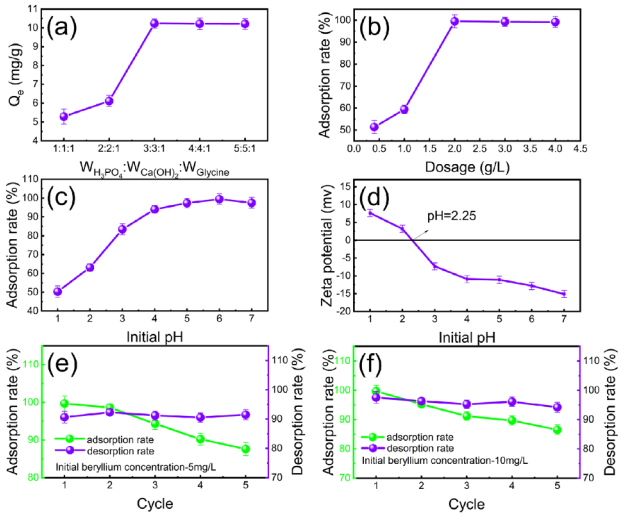

Fig. 2 (Color online) **a** Effect of sample preparation, **b** Influence of adsorbent dosage, **c** Effect of initial pH, **d** Zeta potential, **e** and **f** Adsorption and desorption experiments of CP@Glycine (**e** 5 mg/L, **f** 10 mg/L)

Figure 1c illustrates the FT-IR analysis of CP@Glycine. The bending at 3400 cm^{-1} – 3500 cm^{-1} was mainly attributed to O-H [24–26]. The vibration of the bands at 2900 cm^{-1} and 1650 cm^{-1} is essentially ascribed to the N-H bond [27, 28], whereas the vibration at 1060 cm^{-1} is mainly attributed to the P-OH bond [29]. At 1155 and 1343 cm^{-1}, the characteristic band of in-plane bending of P-O-H has been presented [30]. The vibration of the bands at 890 cm^{-1} and 610 cm^{-1} is essentially attributed to the P-O bond [31].

Figure 1d shows the XRD analysis results of CP@Glycine, revealing multiple characteristic peaks. The presence of $Ca_3(PO_4)_2$ (PDF♯48-0488) leads to the characteristic peak at 2θ=24.2°, 25.6°, 32.2°, while NH_4N_3 (PDF♯09-0499) leads to the characteristic peak at 2θ=29.3° and 38.8°. The obtained results by the SEM, TEM, FT-IR, and XRD revealed that the CP@Glycine sample was successfully prepared.

3.2 Batch experiments

The preparation process of adsorbent significantly affects the adsorption effect. The results of the batch experiments are illustrated in Fig. 2.

Five different ratios were tested for sample preparation ($W_{H_3PO_4}/W_{Ca(OH)_2}/W_{Glycine}$=1:1:1, 2:2:1, 3:3:1, 4:4:1, 5:5:1). The removal efficiency of Be(II) by CP@Glycine is positively correlated with the weight ratio of $W_{H_3PO_4}/W_{Ca(OH)_2}/W_{Glycine}$ and reached the maximum when the weight ratio was 3:3:1 (Fig. 2a). Therefore, the optimal weight ratio of $W_{H_3PO_4}/W_{Ca(OH)_2}/W_{Glycine}$ was 3:3:1.

The amount of absorbent shows the economic benefits of the absorbent material. Figure 2b illustrates the effect of adsorbent dosage. The graph presents that the optimal adsorption rate (99%) is achievable in the case of 2 mg · L^{-1} adsorbent. By this virtue, the adsorbent dosage in this experiment was set as 2 mg · L^{-1}.

The initial pH value of the solution influences the chemical properties and zeta potential of the adsorption process [21]. The plotted results in Fig. 2c reveal that the adsorption rate of Be(II) is positively correlated with increasing pH. The optimum initial pH appears at 6, and the removal efficiency of beryllium reaches 99%. This is because Be(II) mainly exists in the form of $Be_4(OH)_4^{4+}$ for the case of pH>6, which hardly binds to phosphate and ammonia, thus affecting the adsorption efficiency [32]. This phenomenon is also reflected by the zeta site (PH_{zpc}). Figure 2d demonstrates that the PH_{zpc} of CP@Glycine is 2.25. When the pH is lower than PH_{zpc}, the adsorption efficiency is enhanced. The surface of CP@Glycine is positively charged, whereas Be(II) exists as a cation, leading to electrostatic repulsion leading to low adsorption rates [15]. As the pH increases, the deprotonation degree of CP@Glycine gradually decreases. When the surface of CP@Glycine is negatively charged and the phosphate and ammonia groups are likely to form stable complexes with Be(II) [17], the adsorption capacity could be remarkably enhanced, as explained by De [16].

The Be(II) desorption capacity and reusability of CP@Glycine were also studied. Figure 2e–f demonstrates that the removal efficiency of Be(II) decreases slightly, while the desorption rate of beryllium decreases during 5 adsorption–desorption cycles for both 5 mg · L^{-1} beryllium solutions and then remains constant. In the first adsorption and desorption cycle, the removal efficiency of Be(II) is 99% and decreases to 90% (in cycle 3). After 5 cycles, the absorption

rate of Be(II) remains 85%. The results indicate that the desorption rates of Be(II) during 5 cycles are above 90%. Therefore, CP@Glycine has good reusability in the experimental range, which proves that CP@Glycine has economic benefits and acceptable recycling performance.

3.3 Equilibrium modeling

Adsorption kinetics are able to effectively react to the required retention time of the adsorbent. Four kinetic models, namely pseudo-first-order kinetics, pseudo-second-order kinetics, Elovich, and intraparticle diffusion, were used to fit the data of CP@Glycine adsorption of beryllium. Figure 3a–b illustrates the fitting of the adsorption kinetics. The results showed that Be(II) is rapidly absorbed in the initial stage of adsorption. As CP@Glycine occupies many adsorption sites in the early stages, Be(II) is removed in solution [15]. As is seen, the PSO model ($R^2 = 0.999$) is more suitable for fitting the Be(II) removal process by CP@Glycine compared to the PFO model ($R^2 = 0.993$), intraparticle diffusion ($R^2 = 0.921$–0.940), and Elovich ($R^2 = 0.987$–0.996). In addition, the chi-square parameter (χ^2) of the fitted model was lower, and the estimated Q_e values were closer to the experimental data. This suggests that the removal process is regulated by chemisorption and physical adsorption at the same time [16].

Adsorption isotherms were also examined based on the Langmuir model, Freundlich model, Redlich–Peterson model, and Temkin model. Figure 3c illustrates that Q_e and temperature exhibit a positive correlation with the initial concentration of beryllium. The fitting results of the adsorption isotherm models are demonstrated in Fig. 3d–f, and the adsorption isotherm data are listed in Table S2. According to the relevant coefficient (R^2), the Freundlich model ($R^2 = 0.961$) is more suitable for fitting the Be(II) removal process with CP@Glycine for the tested temperature range than the Langmuir model ($R^2 = 0.830$) at 35 °C [13]. At the temperature of 25 °C, the Temkin model ($R^2 = 0.991$) also seems suitable for fitting the adsorption process [32, 33]. By comparing the chi-square parameter (χ^2) of the four equations, it can be seen that the χ^2 values of Langmuir and Temkin at 25 °C are 0.75049 and 0.54103, respectively, which is much lower than that of Freundlich. However, the χ^2 of Freundlich was lower than that of Langmuir and Temkin at 15 and 35 °C. Therefore, the Redlich–Peterson model was introduced, which is a mixture of the Langmuir and Freundlich models [34]. Additionally, the experimental isotherm data fitted by the Redlich–Peterson model revealed that phosphoric acid adsorption on pyrolytic hydrocarbons

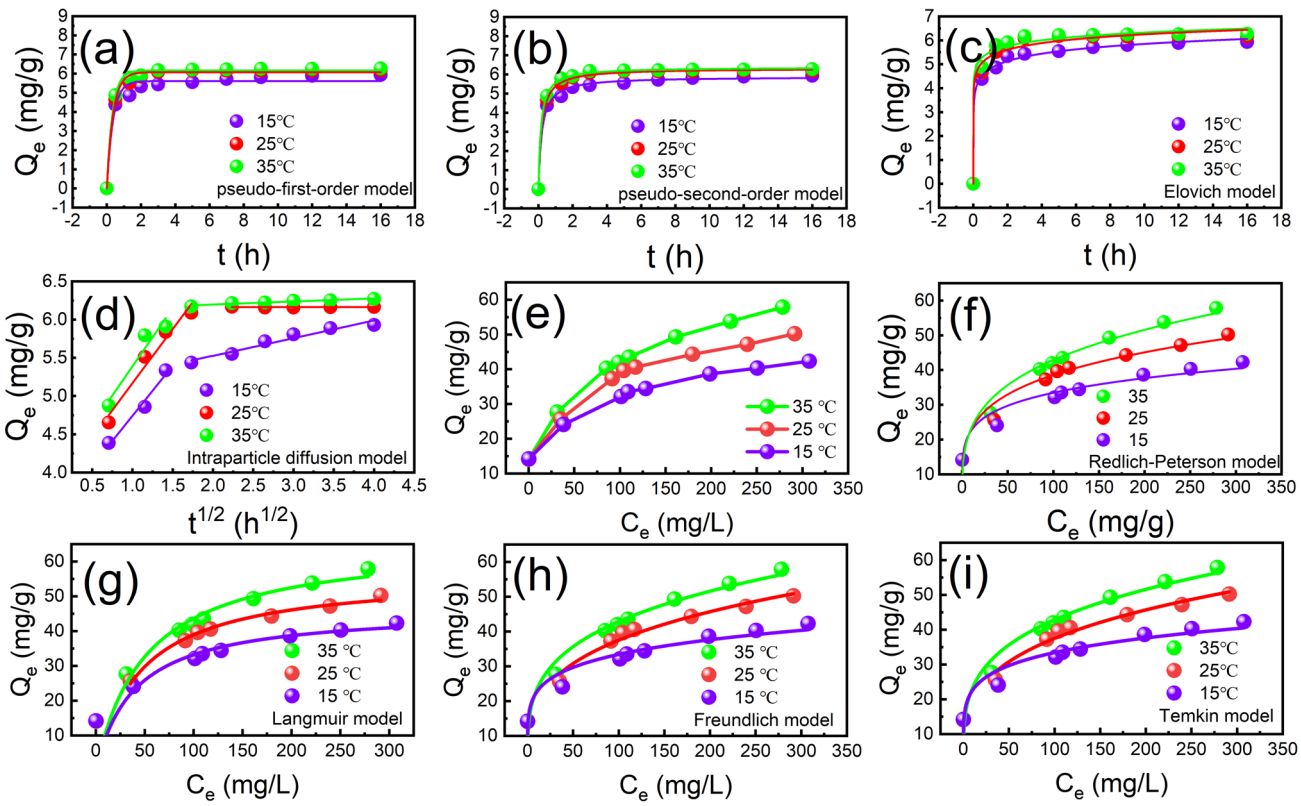

Fig. 3 (Color online) Adsorption kinetics fitting (**a**–**d**), Adsorption isotherm fitting (**e**–**i**)

does not follow the ideal monolayers or heterogeneous surface adsorption, but the mixed adsorption behavior of both. The maximum Q_e of CP@Glycine for beryllium is obtained as 66 mg · g^{-1} at 35 °C. Compared to other adsorbents, CP@Glycine exhibits a higher Q_e for beryllium (Table S3). In addition, the cooperative effect of P-O with N-H and O-H may enhance the removal of beryllium by CP@Glycine.

Adsorption thermodynamics of Be(II) with CP@Glycine was also determined. According to Table S4, during the tested temperature range, the calculated enthalpy change ($\triangle H^0$) is positive (> 0), indicating that the removal progress is associated with a negative heat response [28]. Gibbs free energy ($\triangle G^0$) < 0, indicating that the removal progress is autogenic [21]. Entropy change ($\triangle S^0$) > 0 signifies that the disorder between solid and liquid is increased in the removal progress [35]. To conclude, the removal progress is an autogenous negative heat process, which is consistent with the results of Fig. 3 and Table S4.

3.4 Adsorption selectivity

The selective adsorption experiment of beryllium by CP@Glycine was explored. In U/Be solutions, multiple coexisting ions usually compete for active sites [36]. The separation behaviors of Be(II) with CP@Glycine from the mixed solutions with Zn, Mn, Ca, Fe, Na, and U were also carefully examined. Figure 4a illustrates the competitive adsorption of Be(II) from binary solutions that contain Be(II) and other different metal ions. The obtained results indicate that CP@Glycine exhibits a good adsorption rate (99%) of Be(II) from mixed U/Be solutions with various ion concentrations. The defined distribution coefficient (K_d) shows the adsorption selectivity of Be(II) with CP@Glycine. Figure 4b demonstrates the K_d of each competitor ion at the same concentration. The K_d value of Be(II) with CP@Glycine (K_d=2.53×10^4 mg · L^{-1}) is much higher than the other six elements, which confirms that CP@Glycine has excellent selectivity of Be(II) over other impurities (i.e., Zn(II) (K_d=0.133×10^4 mg · L^{-1}), Mn(II) (K_d=0.023×10^4 mg · L^{-1}), Ca(II) (K_d

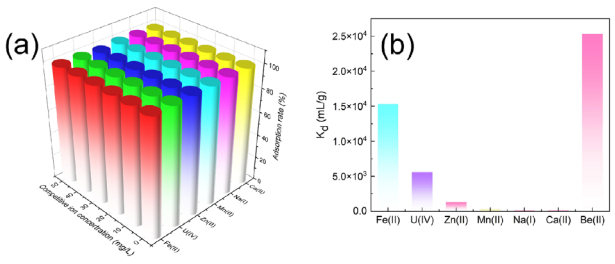

Fig. 4 (Color online) **a** Effect of the coexisting ion concentration on the adsorption rate of beryllium, **b** Effect of the single concentration of coexisting ions on K_d

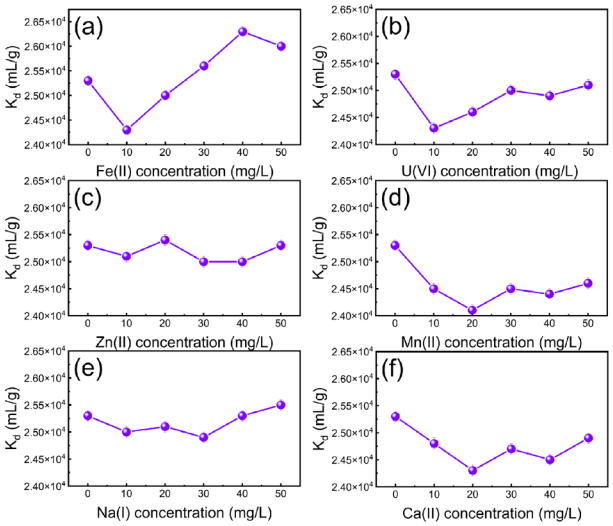

Fig. 5 (Color online) Influence of different coexisting ions on K_d adsorbed by CP@Glycine at different concentrations

=0.014×10^4 mg · L^{-1}), Fe(II) (K_d=1.53×10^4 mg · L^{-1}), Na(I) (K_d=0.013×10^4 mg · L^{-1}), and U(VI) (K_d=0.56×10^4 mg · L^{-1})). To investigate the adsorption selectivity of Be(II) over competitive ions, the influence of different concentrations of competitive ions on K_d of Be(II) was also determined. Figure 5 illustrates the effect of various ion concentrations (i.e., Fe(II), U(VI), Zn(II), Mn(II), Na(I), and Ca(II)) on the K_d value of Be(II). Figure 5a demonstrates that the K_d value of Be(II) grows with increasing Fe(II) concentration because increasing pH may lead to precipitation of Fe(II) and co-precipitation with Be(II) [21]. Figure 5b–f illustrates that within the experimental range, the concentrations of coexisting ions (i.e., Zn, Mn, Ca, Na, and U) have little influence on the K_d value of Be(II). The orders of magnitude of the K_d value of Be(II) are as high as 2.53×10^4 mg · L^{-1}, indicating the strong removal selectivity of CP@Glycine for Be(II) from U/Be solutions.

3.5 Adsorption mechanism

The physical and chemical properties of CP@Glycine before and after adsorption (Used-CP@Glycine) were analyzed by different characterization to discover the adsorption mechanism of Be(II) with CP@Glycine. The surface morphology of CP@Glycine and Use-CP@Glycine is presented in Fig. 6a–f. By comparing the morphology of CP@Glycine and Use-CP@Glycine, many flocs were detected on the surface after adsorption. The energy-dispersive spectrum (EDS) analysis (Fig. 6g) of CP@Glycine and Use-CP@Glycine was further performed. Figure 6h illustrates that the peaks of O element are remarkably increased, indicating that a much amount of O accumulates on Used-CP@Glycine. However,

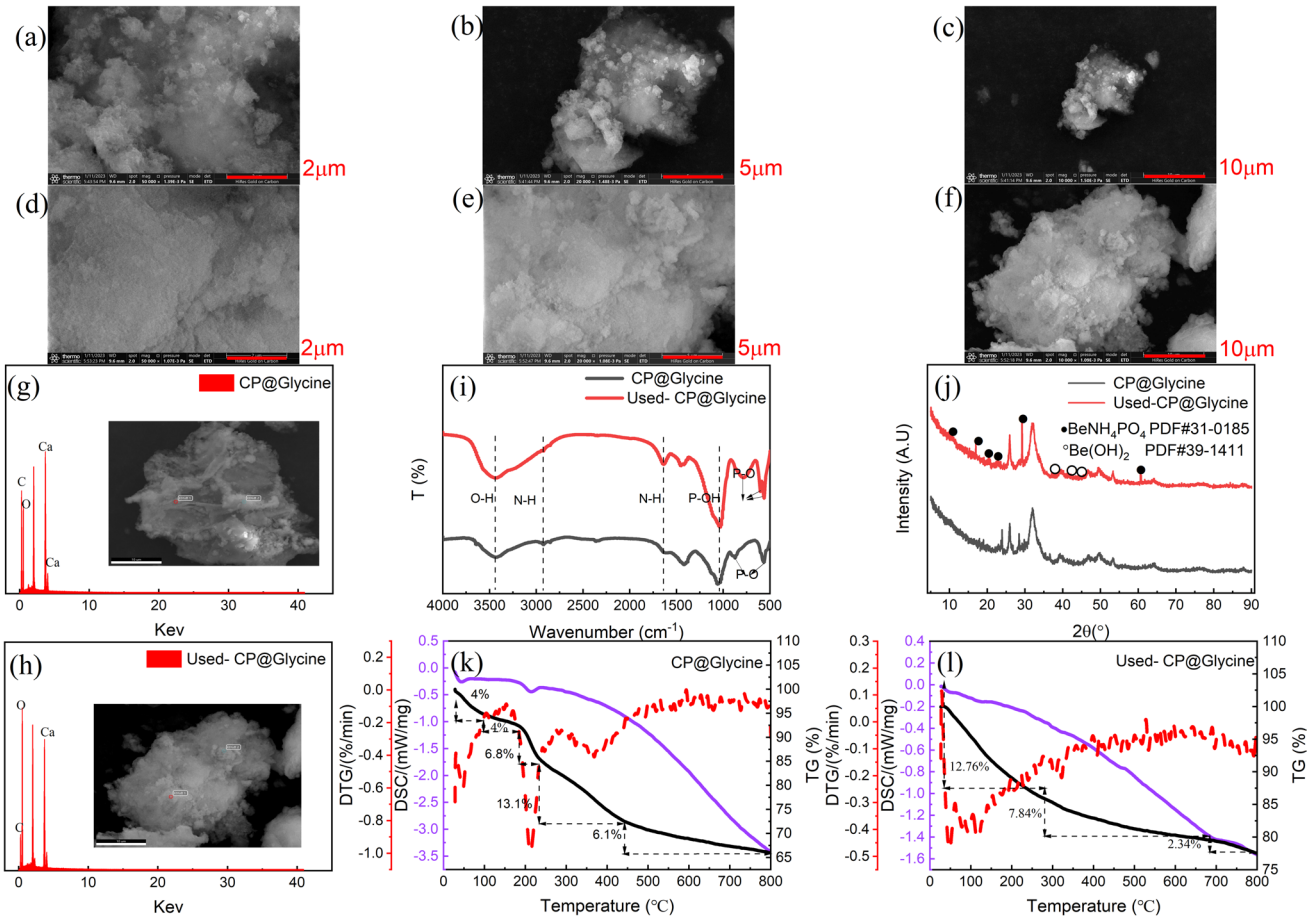

Fig. 6 (Color online) **a–c** SEM images of CP@Glycine, **d–f** Used-CP@Glycine, **g** EDS images of CP@Glycine, **h** Used-CP@Glycine, **i** FT-IR analysis, **j** XRD analysis of CP@Glycine and Used-CP@Glycine, **k** TG analysis of CP@Glycine, **l** TG analysis of Used-CP@Glycine

the Be element peak is not appropriately detected because Be(II) is below the EDS detection line.

The interaction between Be(II) and the adsorbent molecular groups plays a vital role in the removal process [37]. Figure 6i illustrates the FT-IR analysis of CP@Glycine and Use-CP@Glycine. The O-H strength of Use-CP@Glycine increased significantly. CP@Glycine has a strong vibration at 2900 cm^{-1} (N-H), and the vibration becomes weak after adsorption. The N-H bond shifts to 1650 cm^{-1}, which indicates the coordination change of the N-H bond during the reaction process [31] and the formation of a new substance with Be(II). The strength of the P-OH bond enhanced after the reaction in 1060 cm^{-1}, which reveals the increase in the -OH group radical on the CP@Glycine surface. These findings are in reasonable agreement with the EDS results. The removal band at 555 cm^{-1} is essentially designated as the P-O bending from the PO_2^{3-} group [38]. The results indicate that The P-O bond on CP@Glycine was shifted after adsorption, and a new vibration peak of the P-O bond at 690 cm^{-1} appears, which proves that the P-O bond and Be(II) interact to form new products [39].

To characterize the chemical composition of the newly formed product after adsorption, X-ray diffraction (XRD) analysis (Fig. 6j) of CP@Glycine and Use-CP@Glycine was performed before and after adsorption. Figure 6j illustrates that new diffraction peaks appear in the XRD pattern of Use-CP@Glycine compared to the XRD pattern of CP@Glycine, which implies the formation of new products. According to standard diffraction card data, the diffraction peaks of the formed products correspond to $BeNH_4PO_4$ (PDF♯31-0185) and $Be(OH)_2$ (PDF♯39-1411). It can then be concluded that beryllium compounds are produced during the adsorption process and the products are mostly $BeNH_4PO_4$ and $Be(OH)_2$. This finding confirms that the separation of Be(II) is dominated by chemisorption and that both P-O bonds and N-H bonds of CP@Glycine involve the formation of $BeNH_4PO_4$ precipitates. Hence, it is thought that the central Be(II) ion formed a complex due to the presence of two distinct coordinate bonds of CP@Glycine to achieve a chelating effect.

To further confirm the composition of the surface precipitates after adsorption, thermogravimetric analysis (TG) was implemented and the corresponding results of CP@Glycine and Used-CP@Glycine are presented in Fig. 6k–i. The plot associated with CP@Glycine exhibits multiple endothermic peaks, the first peak happens around 65 °C, and the loss value is around 4%, which indicates the lack of water in the adsorption material [40]. The second peak occurs around 200 °C, and the loss value was 6.8%, which was essentially related to the loss of ammonia in CP@Glycine [41]. The third endothermic peak occurs at about 400 °C with a loss value of 13.1%, indicating the dehydroxylation of CP@Glycine [42]. The endothermic loss peak of Used-CP@Glycine is estimated to be 12.76% at about 65 °C–280 °C, which indicates the loss of water and ammonia [41]. The thermogravimetric loss from 300 °C to 690 °C corresponds to the dehydroxylation process of Used-CP@Glycine with a loss of 7.84%. The third endothermic peak appears at the temperature of 700 °C–800 °C, and the loss rate is 2.34%, revealing the conversion process of pyrophosphate ion $P_2O_7^{4-}$ [42].

A previous study has shown that elemental valence changes occur during the adsorption process [31]. Herein, X-ray photoelectron spectroscopy (XPS) (see Fig. 7) has been utilized to analyze the elemental valence changes of CP@Glycine and Used-CP@Glycine C 1 s, O 1 s, N 1 s, and P 2p were further analyzed. Figure 7A illustrates the entire XPS spectrum of CP@Glycine and Used-CP@Glycine. According to Fig. 7B, Be(II) is detected in Used-CP@Glycine, indicating that beryllium is adsorbed to CP@Glycine. Figure 7C demonstrates that the O-C=O bond is converted into a C-O-P bond and a C-OH bond during the reaction, indicating that phosphate is involved in the reaction between Be(II) and CP@Glycine [43, 44]. Compared with CP@Glycine, the area of the $-NH_3^+$ group on Used-CP@Glycine exhibits an obvious growth (Fig. 7D), and the energy shifts. This appropriately interprets the increase in the $-NH_3^+$ group on the surface of Used-CP@Glycine [29] and the participation of such forms. Additionally, the performed analysis shows that the peak at 530.70 eV is considered the O 1 s binding site of the phosphate group (Fig. 7E). The -OH group is added at 532.74 eV on Used-CP@Glycine [45]. Figure 7F demonstrates the analysis of P 2p, and the peak value of P 2p decreases and shifts after adsorption, indicating the formation of complex [46]. The obtained XPS results confirm that the phosphate and amino acids, PO_4^{3-}, NH_4^+, and OH^- of the as-prepared CP@Glycine involve the adsorption of beryllium, which further validates the chelating-like interaction between Be(II) and CP@Glycine.

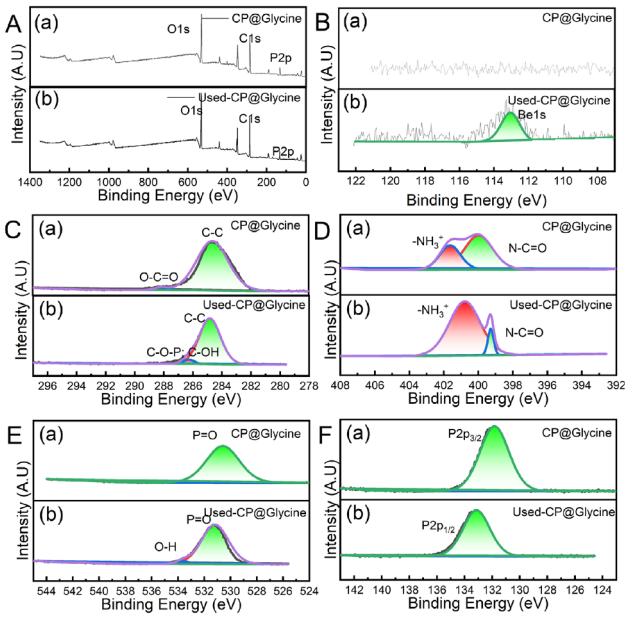

Fig. 7 (Color online) XPS analysis of CP@Glycine and Used-CP@Glycine

3.6 Adsorption mechanism

In this paper, the interaction of Be(II) with a phosphate group and glycine in CP@Glycine has been investigated utilizing the quantum chemistry calculation method. The stable existence forms of glycine, $H_2PO_4^-$, HPO_4^{2-}, and PO_4^{3-} in aqueous solution are shown in Fig. 8.

The optimized structure and binding energy of beryllium and different ligands are presented in Fig. 9.

Figure 9a shows the optimized structures and binding energies of the possible Be(II) complexes formed with glycine. It is found that both the amino and carboxyl groups participate in the bonding with Be^{2+}, the formed complex has the lowest binding energy $-89.24\ kcal \cdot mol^{-1}$, so this binding mode is the most thermodynamically stable [47]. Figure 9b shows the optimized structure and binding energy of Be^{2+} with $H_2PO_4^-$, which shows the binding energy of Be^{2+} and $H_2PO_4^-$ was $-99.92\ kcal \cdot mol^{-1}$. Figure 9c shows the optimized structure of Be^{2+} and HPO_4^{2-}, and the binding energy between Be^{2+} and HPO_4^{2-} is $-145.52\ kcal \cdot mol^{-1}$. In Fig. 9d, the structure of Be^{2+} and PO_4^{3-} is optimized and the binding energy is determined as $-179.97\ kcal \cdot mol^{-1}$. Hence, it can be seen that the binding energy between Be^{2+} and PO_4^{3-} is the lowest as compared with that of the possible Be(II) complexes formed with glycine, indicating that the structure of Be^{2+} and PO_4^{3-} might be the possible thermodynamically stable structure. To further explore the possible chelating structures and binding energies of Be^{2+} with glycine and phosphate ligands, the different Be(II) complexes were optimized and the corresponding binding energies were obtained (Fig. 9e–i). Figure 9e–i shows that among all the composite structures, Gly-Be-PO_4^{3-} (Fig. 9h) has the lowest binding energy, so it is the most thermodynamically stable

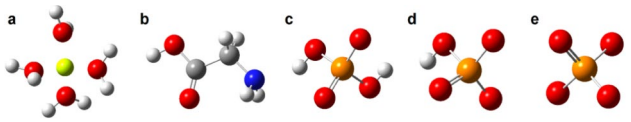

Fig. 8 (Color online) Optimized structures of Be(II) and possible ligands **a** $Be(H^{2+}O)_4^{2+}$, **b** glycine, **c** $H_2PO_4^-$, **d** HPO_4^{2-}, **e** PO_4^{3-}

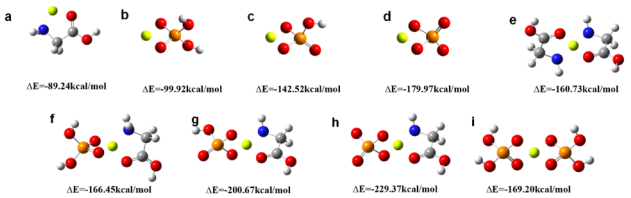

Fig. 9 (Color online) Optimized structures and binding energies of Be^{2+} with different ligands: **a** Be^{2+}-glycine complex, **b** Be^{2+}-$H_2PO_4^-$ complex, **c** Be^{2+}-HPO_4^{2-} complex, **d** Be^{2+}-PO_4^{3-} complex, **e** Be^{2+}- glycine complex, **f** Be^{2+}-$H_2PO_4^-$-glycine complex, **g** Be^{2+}-HPO_4^{2-}-glycine complex, **h** Be^{2+}-PO_4^{3-}-glycine complex, **i** $H_2PO_4^-$-Be^{2+}-$H_2PO_4^-$ complex

in the optimized structure. Therefore, the localized electron density function diagram of the optimized structure is shown in Fig. 10.

Figure 10 presents the electron localized function (ELF) diagram of the electron density distribution among Be, glycine, and phosphate ligands. The cross section of Fig. 10a is the plane where nitrogen/oxygen atoms and Be^{2+} in glycine are located, and the cross section of Fig. 10b is the plane where two oxygen atoms and Be^{2+} directly interacting with Be^{2+} in PO_4^{3-} are located. It can be found that the ELF function value between glycine and Be^{2+} is close to 1, so it can be considered that there is a covalent bond between the glycine and Be^{2+}, and the ELF function value between PO_4^{3-} and Be^{2+} is about 0.8, so there is a covalent bond between the PO_4^{3-} and Be^{2+}. The overlap of electron density among Be, glycine, and phosphate ligands is the maximum for adsorption of Be at the N-O-P site, as shown in Fig. 10a. This is because glycine and PO_4^{3-} have a strong ability to provide electrons, and Be(II) accepts electrons and coordinates with functional groups on the surface of the adsorbent. This indicates that N, O, and P in glycine and phosphate groups provide coordination for Be.

According to the above characterization results, it is speculated that both the N-H bond and P-O bond of CP@Glycine form a stable metal-chelated complex with Be(II) during adsorption [18]. N, O, and P of CP@Glycine all contribute electrons to the coordination of Be^{2+}. The hydroxyl and amino groups of CP@Glycine lead to more anions on the solid surface that produce an electrostatic attraction to positively charged beryllium ions [31]. Moreover, the O-H on

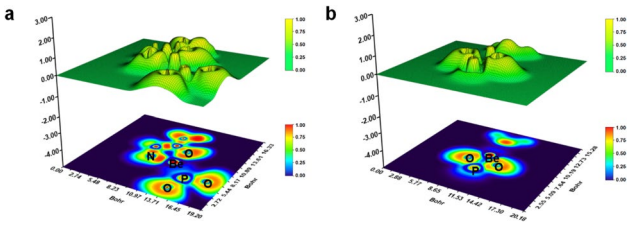

Fig. 10 (Color online) Electron localization density function diagram of Be^{2+} combined with glycine and phosphate ligands

the CP@Glycine combined with Be(II) to form a beryllium hydroxide precipitate [15]. In addition, amino acids have been reported to produce ammonia and phosphate due to the deamination process [47, 48]. These adducts may promote the formation of stable metal chelate complexes with Be(II). The quantum chemical calculation indicates higher stability of Gly-Be-PO_4^{3-} and PO_4^{3-}-Be-PO_4^{3-} than other structures. The higher stability is due to the bonding affinity of beryllium between the PO_4^{3-} and glycine of CP@Glycine. Hence, it can be concluded that the introduction of phosphate and glycine will not only increase the number of active sites on the surface of CP@Glycine but also help in the formation of a stable beryllium complex [36]. To sum up, the selective removal of Be(II) with CP@Glycine is dominated by chemisorption. Further, the occurrence of adsorbents is precipitates of $BeNH_4PO_4$ and $Be(OH)_2$, which show a chelate-like effect during the adsorption process.

4 Conclusion

In this study, first, a chelate-like amino acid/calcium phosphate composite material was designed and synthesized for the efficient, simple, and economic separation of Be(II) from U/Be solutions. According to batch experiments, the best composition for the preparation of CP@Glycine was determined, and the ratio of $W_{H_3PO_4}/W_{Ca(OH)_2}/W_{Glycine}$ (wt/wt/wt) is 3:3:1. The results of adsorption kinetics and thermodynamics show that the maximum Q_e of the adsorption isotherm is 66 mg · g^{-1} at pH 6. Additionally, CP@Glycine exhibited good adsorption and desorption capabilities. After five cycles, the adsorption and desorption efficiencies remained at 85 and 90%, respectively. Furthermore, CP@Glycine demonstrated excellent adsorption selectivity for Be(II). The obtained results revealed that Be(II) can be effectively separated from multicomponent solutions containing Be, Zn, Mn, Ca, Fe, Na, and U. The results of DFT found that the calculated binding energy of the Be complex coordinated with glycine and phosphate (−229.37 kcal · mol^{-1}) was lower than that of other possible Be complexes. The localized electron density function of the Be coordinated complex also verified the tendency to form covalent bonds

between N and O atoms from glycine and P and O atoms from phosphate with Be^{2+}. Furthermore, the chelate-like interaction between Be(II) and CP@Glycine dominates the chemisorption process, and the surface of CP@Glycine has more negative charge and generates electrostatic attraction with beryllium. However, this study was finally only used for the adsorption of beryllium in simulated wastewater. After that, it is necessary to carry out large-scale expansion experiments and consider the recycling of beryllium. These findings guide optimizing the future design of composites based on high beryllium absorption.

Supplementary Information The online version contains supplementary material available at https://doi.org/10.1007/s41365-025-01747-8.

Author Contributions All authors contributed to the study conception and design. Material preparation, data collection, and analysis were performed by Xu Zhao, E-Ming Hu, Yi-Ge Sun, Hao-Shuai Li, Li-Ping Xiang, Hong Liu, Zhi-Wu Lei, Yu-Cheng Su, Bo-Yuan Zheng, Hong-Yang Xia, Khan Muhammad Yaruq Ali, Qing-Liang Wang, and Fang Hu. The first draft of the manuscript was written by Xu Zhao, and all authors commented on previous versions of the manuscript. All authors read and approved the final manuscript.

Data Availability The data that support the findings of this study are openly available in Science Data Bank at https://cstr.cn/31253.11.sciencedb.j00186.00714 and https://www.doi.org/10.57760/sciencedb.j00186.00714.

Declarations

Conflict of interest The authors declare that they have no conflict of interest.

References

1. N. Nikolaus, Beryllium Copper-Beryllium Alloys. Chembioeng. Rev. **5**, 30–33 (2018). https://doi.org/10.1002/cben.201700016
2. Z.Y. Dou, C. Ma, Y.W. Zhao et al., Elevated temperature compressive behavior of a beryllium-aluminum casting alloy. Mater. Lett. **229**, 89–92 (2018). https://doi.org/10.1016/j.matlet.2018.06.067
3. M. Gyoeroek, A. Kaiser, I. Sukuba et al., Surface binding energies of beryllium/tungsten alloys. J. Nucl. Mater. **472**, 76–81 (2016). https://doi.org/10.1016/j.jnucmat.2016.02.002
4. A. Hool, C. Helbig, G. Wierink, Challenges and opportunities of the European Critical Raw Materials Act. Miner. Econ. **37**, 661–668 (2024). https://doi.org/10.1007/s13563-023-00394-y
5. H.N. Qianjian, W.X. Shenyi, K.X. Xing, Soil pollution of beryllium around beryllium smelting plant. J. Liaoning Univers. **S1**, 68–74 (1982)
6. X. Zhao, Q.L. Wang, Y.G. Sun et al., Beryllium adsorption from beryllium mining wastewater with novel porous lotus leaf biochar modified with PO_4^{3-}/NH_4^+ multifunctional groups (MLLB). Biochar **6**, 89 (2024). https://doi.org/10.1007/s42773-024-00385-4
7. Z.Y. Dou, C. Ma, Y.W. Zhao et al., Elevated temperature compressive behavior of a beryllium-aluminum casting alloy. Mater. Lett. **229**, 89–92 (2018). https://doi.org/10.1016/j.matlet.2018.06.067
8. E. Drobyshev, L. Kybarskaya, S. Dagaev et al., New insight in beryllium toxicity excluding exposure to U/Be dust: accumulation patterns, target organs, and elimination. Arch. Toxicol. **93**, 859–869 (2019). https://doi.org/10.1007/s00204-019-02432-7
9. M. Tanveer, L. Wang, Potential targets to reduce beryllium toxicity in plants: a review. Plant. Physiol. Bioch. **139**, 691–696 (2019). https://doi.org/10.1016/j.plaphy.2019.04.022
10. S. Bolan, H. Wijesekara, M. Tanveer et al., Beryllium contamination and its risk management in terrestrial and aquatic environmental settings. Environ. Pollut. **320**, 121077 (2023). https://doi.org/10.1016/j.envpol.2023.121077
11. F. Sun, W.L. Sun, H.M. Sun et al., Biosorption behavior and mechanism of beryllium from aqueous solution by aerobic granule. Chem. Eng. J. **172**, 783–791 (2011). https://doi.org/10.1016/j.cej.2011.06.062
12. M.O. Abd El-Magied, A. Mansour, F.A. Al Ghani. Alsayed et al., Biosorption of beryllium from aqueous solutions onto modified chitosan resin: equilibrium, kinetic and thermodynamic study. J. Dis. Sci. Technol. **39**(11), 1597–1605 (2018). https://doi.org/10.1080/01932691.2018.1452757
13. X. Zhao, Y. Su, H. Wang et al., Modification of activated carbon from agricultural waste lotus leaf and its adsorption mechanism of beryllium. Korean J. Chem. Eng. **40**, 255–266 (2023). https://doi.org/10.1007/s11356-022-23415-9
14. X. Zhao, Y. Su, Z. Lei et al., Adsorptive removal of beryllium by Fe-modified activated carbon prepared from lotus leaf. Environ. Sci. Pollut. R. **30**, 18340–18353 (2022). https://doi.org/10.1007/s11356-022-23415-9
15. X. Zhao, S. Dong, H. Wang et al., Preparation of porous calcium carbonate biochar and its beryllium adsorption performance. J. Environ. Chem. Eng. **11**, 110102 (2023). https://doi.org/10.1016/j.jece.2023.110102
16. G. Eskenazy, Adsorption of beryllium on peat and coals. Fuel **49**, 61–67 (1970). https://doi.org/10.1016/0016-2361(70)90008-6
17. A.D. Sousa, Indirect complexometric determination of beryllium. Talanta **22**, 910–911 (1975). https://doi.org/10.1016/0039-9140(75)80192-5
18. K.R. Krishnamoorthy, R.K. Iyer, Homogeneous precipitation of beryllium by means of trichloroacetic acid hydrolysis and determination as phosphate. Anal. Chim. Acta **47**, 333–338 (1969). https://doi.org/10.1016/S0003-2670(01)95685-5
19. M. Sarvar, Z.S. Tonkaboni, M. Noaparast et al., Application of amino acids for gold leaching: effective parameters and the role of amino acid structure. J. Clean. Prod. **391**, 136123 (2023). https://doi.org/10.1016/j.jclepro.2023.136123
20. J. Zhong, J. Zhou, M. Xiao et al., Design and syntheses of functionalized copper-based MOFs and its adsorption behavior for Pb (II). Chin. Chem. Lett. **33**, 973–978 (2022). https://doi.org/10.1016/j.cclet.2021.07.040
21. P. Wang, E. Hu, Q. Wang et al., Selective extraction of uranium from uranium–beryllium ore by acid leaching. J. Radioanal. Nucl. Ch. **322**, 597–604 (2019). https://doi.org/10.1007/s10967-019-06689-1
22. K. Thanigai Arul, M. Ramesh, C. Chennakesavan et al., Novel multifunctional of magnesium ions (Mg^{++}) incorporated calcium phosphate nanostructures. J. Alloy. Compd. **730**, 31–35 (2018). https://doi.org/10.1016/j.jallcom.2017.09.254
23. B. Li, Y. Wu, W. Zhang et al., Efficient synthesis of amino acid polymers for protein stabilization. Biomater. Sci-UK **7**, 3675–3682 (2019). https://doi.org/10.1039/c9bm00484j
24. A.C. Martins, O. Pezoti, A.L. Cazetta et al., Removal of tetracycline by NaOH-activated carbon produced from macadamia nut shells: kinetic and equilibrium studies. Chem. Eng. J. **260**, 291–299 (2015). https://doi.org/10.1016/j.cej.2014.09.017
25. Y.H. Peng, J.N. Wang, X. Yang et al., Preparation of a novel chelating resin for the removal of Ni^{2+} from water. Chinese Chem. Lett. **25**, 265–268 (2014). https://doi.org/10.1016/j.cclet.2013.11.001

26. Z.M. Elham, L. Taghavi, F. Moeinpour et al., Designing of hydroxyl-terminated triazine-based dendritic polymer/halloysite nanotube as an efficient nano-adsorbent for the rapid removal of Pb (II) from aqueous media. J. Mol. Liq. **360**, 119407 (2022). https://doi.org/10.1016/j.molliq.2022.119407
27. Q. Xin, Q. Wang, J. Gan et al., Enhanced performance in uranium extraction by the synergistic effect of functional groups on chitosan-based adsorbent. Carbohyd. Polym. **300**, 120270 (2023). https://doi.org/10.1016/j.carbpol.2022.120270
28. N.N. Basargin, O.V. Miroshnichenko, Beryllium(II) sorption from aqueous solutions by polystyrene-based chelating polymer sorbents. Russian J. Inorg. Chem. **57**(5), 758–762 (2012). https://doi.org/10.1134/S0036023612050026
29. W. Liu, J. Zhang, C. Zhang et al., Adsorptive removal of Cr (VI) by Fe-modified activated carbon prepared from Trapa natans husk. Chem. Eng. J. **162**, 677–684 (2010). https://doi.org/10.1016/j.cej.2010.06.020
30. Z. Ren, B. Jia, G. Zhang et al., Study on adsorption of ammonia nitrogen by iron-loaded activated carbon from low temperature wastewater. Chemosphere **262**, 127895 (2021). https://doi.org/10.1016/j.chemosphere.2020.127895
31. X. Zhao, Q. Wang, Y. Sun et al., An eco-friendly porous hydrogel adsorbent based on dextran/phosphate/amino for efficient removal of Be (II) from aqueous solution. Int. J. Biol. Macromol. **269**, 131851 (2024). https://doi.org/10.1016/j.ijbiomac.2024.131851
32. I. Polowczyk, A. Bastrzyk, M. Fiedot, Protein-mediated precipitation of calcium carbonate. Materials **9**, 944 (2016). https://doi.org/10.3390/ma9110944
33. K. Wu, B. Wang, B. Tang et al., Adsorption of aqueous Cu (II) and Ag (I) by silica anchored Schiff base decorated polyamidoamine dendrimers: Behavior and mechanism. Chinese Chem. Lett. **33**, 2721–2725 (2022). https://doi.org/10.1016/j.cclet.2021.08.126
34. Z.A. Pezhman, F. Moeinpour, F.S. Mohseni-Shahri, Adsorption isotherm and thermodynamic studies of As (III) removal from aqueous solutions using used cigarette filter ash. Appl Water Sci **9**, 172 (2019). https://doi.org/10.1007/s13201-019-1059-9
35. A.M. Arafat, C. Chambers, M.T. Reza et al., Application of corn stover derived pyrolyzed hydrochars for efficient phosphorus removal from water: Influence of pyrolysis temperature. Chem. Eng. J. Adv. **18**, 100613 (2024). https://doi.org/10.1016/j.ceja.2024.100613
36. Y.W. Cai, L. Chen, S.T. Yang et al., Rational synthesis of novel phosphorylated chitosan- carboxymethyl cellulose composite for highly effective decontamination of U(VI). ACS Sustain. Chem. Eng. **7**, 5393–5403 (2019). https://doi.org/10.1016/j.apsusc.2019.04.103
37. Y. Liao, M. Wang, D.J. Chen, Electrosorption of uranium (VI) by highly porous phosphate-functionalized graphene hydrogel. Appl. Surf. Sci. **484**, 83–96 (2019). https://doi.org/10.1016/j.apsusc.2019.04.103
38. Y. Tian, L.J. Liu, F.Q. Ma et al., Synthesis of phosphorylated hyper-cross-linked polymers and their efficient uranium adsorption in water. J. Hazard. Mater. **419**, 126538 (2021). https://doi.org/10.1016/j.jhazmat.2021.126538
39. X. Zhang, L. Zhang, Q. Wang et al., Selective, rapid extraction of uranium from aqueous solution by porous chitosan-phosphorylated chitosan-amidoxime macroporous resin composite and differential charge calculation. Int. J. Biol. Macromol. **253**, 126661 (2023). https://doi.org/10.1016/j.ijbiomac.2023.126661
40. N. Laohavisuti, B. Boonchom, W. Boonmee et al., Simple recycling of biowaste eggshells to various calcium phosphates for specific industries. Sci. Rep-UK **11**, 15143 (2021). https://doi.org/10.1038/s41598-021-94643-1
41. G. Zhang, H. Wu, Z. Peng et al., TG/DTA and XRD study on structure and chemical transformation of the Cs–P–W oxides. J. Therm. Anal. Calorim. **128**, 947–956 (2017). https://doi.org/10.1007/s10973-016-5990-9
42. M. Jamil, A. Elouahli, H. Khallok et al., Characterization of β-tricalcium phosphate-clay mineral composite obtained by sintering powder of apatitic calcium phosphate and montmorillonite. Surf. Interfaces **17**, 100380 (2019). https://doi.org/10.1016/j.surfin.2019.100380
43. Z.W. Huang, Z.J. Li, L.R. Zheng et al., Interaction mechanism of uranium(VI) with three-dimensional graphene oxide-chitosan composite: Insights from batch experiments, IR, XPS, and EXAFS spectroscopy. Chem. Eng. J. **328**, 1066–1074 (2017). https://doi.org/10.1016/j.cej.2017.07.067
44. W. Qiao, P. Zhang, L. Sun et al., Adsorption performance and mechanism of Schiff base functionalized polyamidoamine dendrimer/silica for aqueous Mn (II) and Co (II). Chin. Chem. Lett. **31**, 2742–2746 (2020). https://doi.org/10.1016/j.cclet.2020.04.036
45. Z.B. Zhang, Z.M. Dong, X.X. Wang et al., Synthesis of ultralight phosphorylated carbon aerogel for efficient removal of U(VI): batch and fixed-bed column studies. Chem. Eng. J. **370**, 1376–1387 (2019). https://doi.org/10.1016/j.cej.2019.04.012
46. E.A. Imam, E.-T.I. El-Sayed, M.G. Mahfouz et al., Synthesis of α-aminophosphonate functionalized chitosan sorbents: Effect of methyl vs phenyl group on uranium sorption. Chem. Eng. J. **525**, 1022–1034 (2018). https://doi.org/10.1016/j.cej.2018.06.003
47. J. Kohn, S. Spicher, M. Bursch et al., Quickstart guide to model structures and interactions of artificial molecular muscleswith efficient computational methods. Chem. Commun. **58**, 258–261 (2021). https://doi.org/10.1039/D1CC05759F
48. M. Szabó, V. Bíró, F. Simon et al., The decomposition of *N*-chloro amino acids of essential branched-chain amino acids: kinetics and mechanism. J. Hazard. Mater. **382**, 120988 (2020). https://doi.org/10.1016/j.jhazmat.2019.120988